

64. OPAQUE MINERALS IN BASALTS FROM HOLES 417D AND 418A

A. D. Genkin, I. P. Laputina, and N. N. Pertsev,
Institute of Geology of the Ore Deposits, Petrography, Mineralogy, and Geochemistry,
USSR Academy of Sciences, Moscow, USSR

INTRODUCTION

Opaque minerals constitute an important part of the basalts under study. Analysis of opaque minerals can provide a fuller understanding of some processes during congelation of basalts, as well as on the peculiarities of low-temperature alteration of basalts. Although this investigation is limited to consideration of 27 specimens (Table 1), its results reflect main features of the ore mineralogy at Sites 417 and 418.

The assemblages of opaque minerals in basalts, the composition of individual minerals, and their grain sizes depend chiefly on two factors: (1) the rate of cooling which determines the grain size of rock-forming and opaque minerals, and the texture of the rocks; and (2) the degree of secondary alteration. There is distinct correlation between degree of alteration and grain size. The coarser grained basalts are found in fresher rocks; fine-grained basalts usually are quite altered. The primary and secondary opaque mineral assemblages distribution also depends upon this regularity.

We have found the following primary opaque minerals in basalts: titanomagnetite, ilmenite, chromite, pyrrhotite, chalcopyrite, and pentlandite. The most widespread secondary opaque mineral is pyrite. Chalcopyrite, marcasite, and iron hydroxides were also noted.

We have observed primary sulfides only in less-altered coarse-grained basalts (Samples 417D-69-1, 142 cm and 418A-85-1, 33 cm); altered basalts contain only pyrite and chalcopyrite.

PRIMARY OPAQUE MINERALS

Titanomagnetite

Titaniferous magnetite is the most widespread opaque mineral in the basalts studied. The groundmass of basalts (predominately fine-grained with plagioclase, olivine, and pyroxene phenocrysts) contains numerous, very small (20 to 50 μm) skeletal magnetite crystals (Plate 1, Figures 1 and 2). One can see the delicate form of these crystals at great magnifications. Very minute grains ($<1 \mu\text{m}$) of magnetite are present adjacent to these skeletal crystals (Plate 1, Figure 2). Magnetite phenocrysts are very rare in the basalts and occur in small euhedral grains up to 100 μm .

These correlations suggest that the precipitation of magnetite from basalt melt began simultaneously with the formation of silicate phenocrysts and ended with consolidation of the groundmass. Minute magnetite grains, ranging in size from 1 to 7 μm , occur in coarse-grained basalts, too. They are located in interstitial fine-grained mesostasis be-

tween coarse grains of plagioclase, pyroxene, olivine, and magnetite (Plate 1, Figure 3). Rounded, elongated, locally euhedral forms of these fine grains of magnetite are observable under magnification (Plate 1, Figure 4).

Fine-grained skeletal magnetite grains frequently form crescentic fillings around small vesicles (Plate 2, Figure 1a, b) possibly due to a flotation effect. The meniscus of such fillings have the same orientation in thin section, giving evidence of their origin in liquid groundmass.

Larger (1 mm and more) euhedral magnetite grains are characteristic for coarse-grained basalts (Samples 417D-67-7, 74 cm; 417D-69-1, 142 cm; 418A-79-1, 113 cm; and 418A-85-1, 33 cm). They occur preferentially along the grain boundaries of plagioclase and pyroxene (Plate 2, Figure 2). The biggest magnetite grains, which sometimes are located in mesostasis, have skeletal forms (Plate 2, Figure 3) and contain inclusions of solidified residual basalt melt. Smaller skeletal magnetite crystals, with minute ($\sim 1 \mu\text{m}$) sulfide globules adhered (Plate 2, Figure 4), are also found in the mesostasis.

The optic investigation of the coarse-grained magnetite at magnifications of 500 to 1000 \times shows that there are lamellar ilmenite intergrowths, sometimes up to 5 to 7 μm across (Plate 3, Figure 1). Thicker ilmenite plates are rare (Plate 3, Figure 2). Most commonly, the width of the plates does not exceed 1 to 2 μm (Plate 3, Figure 3).

Investigators of Mid-Atlantic Ridge (MAR) basalts recovered during DSDP Leg 37 (Wayman and Evans, 1977; Hall and Fisher, 1977) have pointed out the lack of ilmenite in the magnetites, when compared to terrestrial basalts with ilmenite-magnetite intergrowths. Wayman and Evans (1977) have not found any compositional inhomogeneity in dendritic magnetite grains, even at 10,000 \times magnification under an electron microscope, and have concluded that the lack of ilmenite in submarine basalts results from the characteristics of their cooling and oxidation. Earlier studies of dredged MAR basalts (Carmichael, 1970) have shown, however, that coarse-grained varieties usually contain magnetite-ilmenite intergrowths and even separate ilmenite grains.

We have determined the composition of titanomagnetites, as well as other opaque minerals, by means of electron microprobe analysis. Microprobe analysis results for both fine skeletal and large titanomagnetite grains without optically visible ilmenite inclusions are given in Table 2. Abnormal sums and rather high SiO_2 , Al_2O_3 , and MgO contents in minute skeletal magnetites appear to be connected with the capture of adjacent silicates by the microprobe.

TABLE 1
Basalt Samples Selected for Opaque Mineralogy Study

Sample (Interval in cm)	Unit	Rock Type	Opaque Minerals
417D-48-6, 86	8a	Medium-grained, moderately altered basalt with phenocrysts of plagioclase and olivine	Titanomagnetite ^{ab} Pyrite Chalcopyrite
417D-49-1, 69	8b	Medium-grained, moderately altered basalt with phenocrysts of plagioclase and olivine	Titanomagnetite ^a Pyrite
417D-49-2, 82	8b	Medium-grained, moderately altered basalt with phenocrysts of plagioclase and olivine	Titanomagnetite ^a Iron hydroxides
417D-50-1, 95	8b	Fine-grained, moderately altered basalt with phenocrysts of plagioclase, pyroxene, and olivine	Titanomagnetite ^a Iron hydroxides Pyrite
417D-52-4, 13	9a	Fine-grained, moderately altered basalt with phenocrysts of plagioclase, pyroxene, and olivine	Titanomagnetite ^a Pyrite Marcasite
417D-54-5, 46	9a	Fine-grained, moderately altered basalt with phenocrysts of plagioclase, pyroxene, and olivine	Titanomagnetite ^a Pyrite Marcasite Chalcopyrite
417D-59-3, 104	9b	Fine-grained, moderately altered basalt with phenocrysts of plagioclase, pyroxene, olivine	Titanomagnetite ^a Pyrite Chalcopyrite
417D-62-4, 58	9	Fine-grained, moderately to badly altered basalt with phenocrysts of plagioclase, pyroxene and olivine	Titanomagnetite ^a
417D-63-5, 24	9	Fine-grained, moderately to badly altered basalt with phenocrysts of plagioclase, pyroxene and olivine	Pyrite Chalcopyrite
417D-64-3, 33	9	Fine-grained, moderately to badly altered basalt with phenocrysts of plagioclase, pyroxene and olivine	Pyrite
417D-64-4, 99	10a	Fine-grained, moderately to badly altered basalt with phenocrysts of plagioclase, pyroxene and olivine	Titanomagnetite ^a Pyrite Chalcopyrite
417D-66-5, 123	11	Fine-grained, moderately to badly altered basalt with phenocrysts of plagioclase, pyroxene and olivine	Titanomagnetite ^a Pyrite
417D-67-3, 11	12	Fine-grained, moderately to badly altered basalt with phenocrysts of plagioclase, pyroxene and olivine	Titanomagnetite ^a Pyrite Chalcopyrite
417D-67-7, 74	13	Medium-grained phyric basalt, moderately altered with phenocrysts of plagioclase	Titanomagnetite ^b Ilmenite Pyrrhotite ^c Pyrite Chalcopyrite
417D-69-1, 142	13	Medium-grained phyric basalt, moderately altered with phenocrysts of plagioclase	Titanomagnetite ^b Ilmenite Pyrrhotite Chalcopyrite
418A-57-4, 136	8c	Fine-grained badly altered basalt with phenocrysts of plagioclase and olivine	Titanomagnetite ^a Pyrrhotite + Chalcopyrite ^d Pyrite
418A-58-1, 8	8c	Fine-grained badly altered basalt with phenocrysts of plagioclase and olivine	Titanomagnetite ^a Pyrite
418A-58-4, 143	8c	Fine-grained badly altered basalt with phenocrysts of plagioclase and olivine	Pyrite
418A-68-2, 108	13	Fine-grained, moderately altered basalt with phenocrysts of plagioclase, pyroxene and forsterite	Titanomagnetite ^a Pyrite Chalcopyrite
418A-69-1, 57	13	Fine-grained, moderately altered basalt with phenocrysts of plagioclase, pyroxene and forsterite	Titanomagnetite ^a Pyrite Chalcopyrite
418A-69-3, 139	13	Fine-grained, moderately altered basalt with phenocrysts of plagioclase, pyroxene and forsterite	Titanomagnetite ^a Pyrite
418A-69-5, 99	13	Fine-grained, moderately altered basalt with phenocrysts of plagioclase, pyroxene and forsterite	Titanomagnetite ^a Pyrite Chalcopyrite

TABLE 1 – Continued

Sample (Interval in cm)	Unit	Rock Type	Opaque Minerals
418A-74-4, 90	13	Fine-grained, moderately altered basalt with phenocrysts of plagioclase, pyroxene and forsterite	Titanomagnetite ^a Pyrite
418A-77-1, 87	14b	Aphyric fine-grained basalt, moderately altered	Pyrite
418A-79-1, 113	14b	Coarse-grained basalt aphyric, moderately altered	Titanomagnetite ^{a, b} Pyrite
418A-79-6, 60	14b	Coarse-grained basalt aphyric, moderately altered	Titanomagnetite ^a Pyrrhotite ^c Chalcopyrite ^f
418A-85-1, 33	14c	Coarse-grained basalt aphyric, moderately altered	Chromite Titanomagnetite ^b + ilmenite Ilmenite Pyrrhotite Chalcopyrite Cubanite Pentlandite

^aMinute skeletal and point-grains of titanomagnetite.

^bCoarse grains of titanomagnetite, locally with ilmenite lamellae.

^cOne globule (40 μm) in phenocryst of plagioclase.

^dRare inclusions in phenocrysts of plagioclase.

^eRare, minute (1 to 5 μm) globules in the mesostasis.

^fIntergrowth of chalcopyrite and pyrrhotite in a coarse grain of plagioclase.

We recalculated total iron in the titanomagnetite and ilmenite analyses using the techniques described by Carmichael (1967).

The distinct feature of all titanomagnetites studied is high ulvospinel content. This conclusion is supported by X-ray investigation. Unit cell size obtained, $a = 8.47\text{\AA}$, is close to the ulvospinel unit cell.

A very thin inclusion in a magnetite grain of Sample 417D-69-1, 142 cm was found during the microprobe analyses. It consists of the following: FeO (total) = 8.55, TiO₂ = 63.0, Cr₂O₃ = 0.97, MgO = 4.05, MnO = 0.1, SiO₂ = 9.4, Al₂O₃ = 2.0, and V₂O₅ = 1.1, for a total of 89.14 weight per cent.

Ilmenite

We observed ilmenite only in coarse-grained basalts. It occurs as lamellar inclusions in titanomagnetite grains (Plate 3, Figures 1 to 3). Minute separate grains of ilmenite are found by microprobe investigation in the fine-grained interstitial mesostasis of the basalts.

We determined the composition of the lamellar ilmenites and the titanomagnetite matrix. The microprobe analyses of four co-existing titanomagnetite-ilmenite pairs are given in Table 3. Mole percents of ulvospinel in magnetite and $R_2O_3 = Fe_2O_3 + V_2O_3 + Cr_2O_3 + Al_2O_3$ in ilmenite also are listed in Table 3. Minor element distribution within these co-existing pairs shows that titanomagnetite contains more vanadium and aluminum, and less magnesium in comparison with ilmenite.

Experimental data (Buddington and Lindsley, 1964) give an opportunity to evaluate temperature and oxygen fugacity in equilibrium in magnetite-ilmenite pairs. These values, obtained from the Buddington and Lindsley diagram as well as data from the corrected diagram (Poltavets, 1975), are provided in Table 3. Titanomagnetite exsolution in coarse-grained basalts confirms lower rates of cooling as compared to basalts with fine-grained groundmass. Lack of exsolution phenomena in the skeletal magnetite crystals found in interstitial mesostasis of the coarse-grained basalts (Plate 2, Fig-

TABLE 2
Microprobe Analyses of Titanomagnetite

Sample (Interval in cm)	Minute Skeletal and Point Grains of Titanomagnetite						Coarse Grains of Titanomagnetite						
	417D-49-2, 82			418A-79-1, 113			417D-69-1, 142				418A-79-1, 113		418A-85-1, 33
Analysis No.	1	2	3	1	1	1	1	2	3	4	2	1	2
Compounds Analyzed													
V ₂ O ₅	0.40	0.96	0.42	0.11	0.85	0.92	0.66	0.56	0.66	0.31	0.76	0.76	0.76
SiO ₂	4.1	2.0	5.2	9.36	0.5	1.29	0.55	0.68	0.61	1.64	0.65	0.62	0.62
TiO ₂	18.0	15.8	17.3	17.43	22.5	21.37	21.24	20.97	21.31	20.98	19.19	17.40	17.40
Al ₂ O ₃	3.9	3.5	4.6	2.08	1.8	1.65	1.34	1.79	1.27	1.36	1.49	1.67	1.67
Cr ₂ O ₃	—	—	—	0.47	—	0.30	0.33	0.30	0.29	0.53	0.19	0.20	0.20
Fe ₂ O ₃	—	—	—	—	—	21.66	24.06	23.47	23.68	21.16	29.48	30.45	30.45
FeO	63.97	66.13	67.48	67.45	—	50.07	49.35	49.07	49.50	51.26	47.56	44.61	44.61
MnO	0.54	0.8	0.3	1.37	0.73	0.73	0.90	0.81	0.77	1.62	0.76	0.73	0.73
MgO	3.4	4.0	0.5	0.16	0.5	1.15	0.76	0.92	0.76	0.28	1.37	1.49	1.49
NiO	—	—	—	0.24	—	0.04	0.04	0.08	0.07	0.31	0.01	0.07	0.07
Total	94.21	93.69	95.8	98.65	—	99.29	99.34	98.75	99.02	99.45	101.60	98.00	98.00
Mol. % ulvospinel	—	—	—	—	—	61.4	59.3	58.7	60.1	63.1	52.7	49.2	49.2

Note: In Analyses 1, 2, and 3 of Sample 417D-49-2, 82 cm and Analysis 1 of Sample 418A-79-1, 113 cm, the total iron is represented as FeO. High content of Si, Mg, and Al in these analyses appears related to minute silicate inclusions.

TABLE 3
Microprobe Analyses of Coexisting Titanomagnetites and Ilmenites

Sample (Interval in cm)	417D-69-1, 142			418A- 85-1, 33	
	1	2	3	1	1
Compounds Analyzed					
Titanomagnetite					
V ₂ O ₅	1.06	0.97	1.3	1.44	1.44
SiO ₂	0.48	0.71	0.39	1.05	1.05
TiO ₂	21.6	21.3	19.6	15.52	15.52
Al ₂ O ₃	2.4	1.82	2.9	3.16	3.16
Cr ₂ O ₃	0.37	0.31	0.37	0.15	0.15
Fe ₂ O ₃	17.64	22.17	22.43	19.56	19.56
FeO	53.02	49.57	49.78	50.85	50.85
MnO	0.59	0.75	0.45	0.56	0.56
MgO	1.23	0.92	1.5	3.13	3.13
NiO	—	—	—	0.08	0.08
Total	98.39	98.52	98.72	95.51	95.51
Mol. % ulvospinel	64.4	59.5	53.6	52.0	52.0
Ilmenite					
V ₂ O ₅	0.32	0.38	0.37	0.60	0.43
SiO ₂	0.63	1.0	0.79	0.81	0.27
TiO ₂	48.22	48.03	48.14	48.5	50.3
Al ₂ O ₃	0.29	0.33	0.33	0.42	0.26
Cr ₂ O ₃	0.35	0.33	0.33	0.35	0.35
Fe ₂ O ₃	7.58	8.76	8.14	6.0	4.39
FeO	39.01	38.29	39.08	40.9	41.74
MnO	0.63	0.59	0.63	0.82	0.47
MgO	2.49	3.16	2.53	1.56	1.69
NiO	0.06	0.04	0.10	—	—
Total	99.58	101.02	100.54	99.96	99.96
Mol. % R ₂ O ₃	8.1	8.9	8.7	7.1	5.2
T [°] C ^a	1050	—	960	920	940
log fO ₂ ^a	-11.0	—	-11.8	-12.4	-12.2
T [°] C ^b	1100	—	1035	980	1030
log fO ₂ ^b	-10.0	—	-10.4	-11.8	-11.8

^aAfter Buddington and Lindsley (1964).

^bAfter Poltavets (1975).

ure 4) indicates that their formation was later than the crystallization of larger magnetite grains and that the temperature of fine-grained skeletal magnetite crystallization was equal to exsolution temperature of the coarse magnetite grains.

Chromite

Chromium spinel is not a rare mineral of the basalts discussed; rather, it is abundant, especially in Unit 6b of Hole 418A (see Site 418 Report, this volume). It occurs there not only as minute inclusions, but also as rare small phenocrysts. However, in the specimens studied here (Table 1), we found it only in the coarse-grained aphyric basalt (Sample 418A-85-1, 33 cm). There were only five minute spinel grains in the entire polished section, and all were located in two neighboring, partly altered olivine phenocrysts (Plate 3, Figure 4). The spinel grains are included in smectite pseudomorphs after olivine and have different shapes and sizes. One of them (Plate 3, Figure 4, Grain 1) is angular with dimensions of 50 by 100 μ m. The other spinel grains are rounded and about 40 μ m across; some include very fine, rounded silicate grains.

Microprobe analyses of four of the spinel grains (Table 4) have demonstrated significant differences in their composition. Three types can be distinguished by Fe-Al-Mg relations. The first type (identified as Grain 1) has high FeO + Fe₂O₃ and low Al₂O₃ and MgO contents. Another type is noted for low iron and high alumina and magnesia contents (Grain 4). The third type is intermediate (Grains 2 and 3). We found no composition zonality in the grains, as opposed to the zonal spinels from basalts and peridotites recovered in Leg 37 (Sigurdsson, 1977).

Chemical distinctions of the neighboring spinel grains indicate that there was a time sequence in their crystalliza-

TABLE 4
Microprobe Analyses of Chromospinel From Sample 418A-85-1, 33 cm

Grain No.	1						2			3			4		
	Analytical Focus														
Compounds	Center	Upper rim	Lower rim	Center	Upper rim	Lower rim	Center	Upper rim	Center	Upper rim	Lower rim	Center	Upper rim	Lower rim	
V ₂ O ₅	0.11	0.13	0.1	0.15	0.28	0.2	0.08	0.15	—	—	—	—	—	—	
SiO ₂	0.85	1.9	0.86	0.83	0.83	0.8	0.86	0.87	1.0	0.88	0.9	—	—	—	
TiO ₂	1.2	1.1	2.1	0.58	0.65	0.6	0.50	0.55	—	—	—	—	—	—	
Al ₂ O ₃	18.4	17.1	15.5	20.2	20.7	20.3	20.2	19.9	31.0	32.2	31.7	—	—	—	
Cr ₂ O ₃	34.8	34.3	33.7	36.6	38.4	37.0	36.2	37.2	31.1	31.0	31.3	—	—	—	
Fe ₂ O ₃	13.0	11.4	13.9	11.4	9.6	12.2	11.3	9.9	8.9	6.6	8.8	—	—	—	
FeO	23.9	21.6	22.4	17.9	18.5	17.7	18.1	17.0	13.1	13.2	13.7	—	—	—	
MgO	7.5	8.1	8.1	11.0	11.1	11.0	10.7	11.2	15.5	15.3	15.5	—	—	—	
MnO	0.61	0.55	0.57	0.48	0.48	0.52	0.53	0.55	0.35	0.33	0.33	—	—	—	
NiO	0.05	—	—	0.07	—	—	0.11	0.1	0.06	0.05	0.06	—	—	—	
Total	100.4	96.2	97.2	99.2	100.6	100.3	98.6	97.4	101.0	99.6	102.3	—	—	—	
Mg/Mg+Fe ²⁺ (mol)	0.36	0.401	0.392	0.524	0.518	0.525	0.513	0.540	0.677	0.673	0.669	—	—	—	
Cr/Cr+Al	0.559	0.574	0.593	0.549	0.555	0.550	0.546	0.556	0.402	0.392	0.398	—	—	—	
Fe ³⁺ /Fe ³⁺ +Cr+Al	0.166	0.154	0.189	0.140	0.116	0.147	0.140	0.123	0.099	0.074	0.096	—	—	—	

tion. The angular chromite grains seem to be formed later than the others, at increasing oxygen fugacity in the melt. However, the data are insufficient for well-founded conclusions.

Comparison between spinel compositions determined here and spinels of MAR basalts, gabbros, and peridotites (Sigurdsson, 1977; Clarke and Loubat, 1977; Symes et al., 1977) is given in the Fe³⁺/Fe³⁺ + Cr + Al versus Mg/Mg + Fe²⁺ diagram (Figure 1). Significant differences between them are accountable by the fact that the composition field of the spinels from lavas and peridotites of Leg 37 is within the spinel field from alpine peridotites, while only Grain 4 from Sample 418A-85-1, 33 cm is within the spinel field. Compositions of Grains 2 and 3 are in the spinel field from Bushveld and Stillwater stratiform intrusives. Compositions of Grain 1 are outside even the last field. Mg/Mg + Fe²⁺ values in olivines of Sample 418A-85-1, 33 cm vary from 0.83 to 0.89. Our olivine-chromite pairs fell within the Stillwater field in the Fe²⁺ versus Mg distribution diagram (Sigurdsson, 1977) distal from the MAR basalts field.

Sulfides

Primary sulfide aggregates consisting mainly of pyrrhotite with subordinate chalcopyrite, cubanite, and minor to rare pentlandite occur almost exclusively in fresher coarse-grained basalts (Samples 417D-69-1, 142 cm and 418A-85-1, 33 cm). It is important to note the following features of these sulfides.

- 1) Globular or ellipsoidal forms, from 10 to 100 μ m across, are very characteristic (Plate 4, Figures 1 and 2).
- 2) Sulfide globules are found predominately in fine-grained interstitial mesostasis located between coarse grains of plagioclase, clinopyroxene, and olivine (Plate 4, Figure 1).
- 3) Primary sulfide aggregates are subordinate to titanomagnetite aggregates (Plate 4, Figure 3). There are semi-spherical growths of sulfides on titanomagnetite grains (Plate

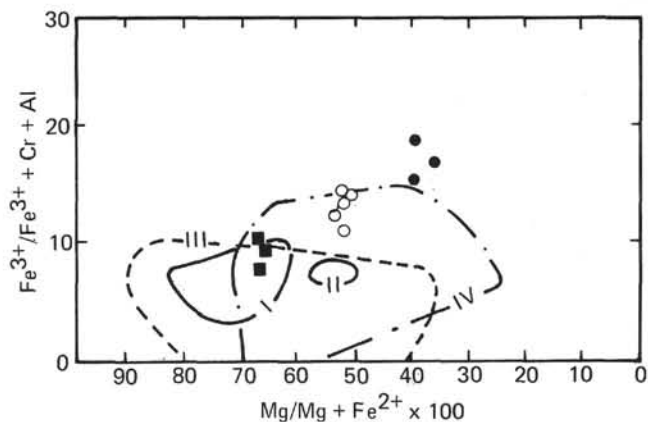


Figure 1. Diagram of Mg/Mg+Fe²⁺ versus Fe³⁺/Fe³⁺+Al+Cr for chromites from Sample 418A-85-1, 33 cm and other chromite mineralization occurrences. The compositions of chromites from Sample 418A-85-1 (Table 4): filled circles = grain 1; open circles = grains 2 and 3; filled squares = grain 4. The composition fields of spinels: I – from Leg 37 basalts (Sigurdsson, 1977), II – from Leg 37 peridotites (Sigurdsson, 1977), III – from alpine peridotites (Irvine, 1967), IV – from the Stillwater and Bushveld layered igneous complexes (Irvine, 1967).

4, Figure 4), indicating later formation of sulfides in comparison with coarse magnetite grains.

- 4) Sulfide aggregates contain minute inclusions of basalt glass.
- 5) Sulfide aggregates occur as intergrowths of different sulfide minerals and as homogeneous masses.

In addition to the sulfides found in Samples 417D-69-1, 142 cm and 418A-85-1, 33 cm, primary sulfides have been found as minute spherical pyrrhotite and pyrrhotite-chalcopyrite inclusions in plagioclase phenocrysts (Samples 417D-67-7, 74 cm; 418A-57-4, 136 cm; and 418A-79-6, 60 cm). Primary sulfides in the studied samples of basalts with

fine-grained groundmass are usually absent, unlike the widespread distribution of sulfide globules in the Leg 37 basalts (Hall and Fisher, 1977). This scarcity seems to be connected with the more intensive alteration of the Leg 51-53 fine-grained basalts.

Pyrrhotite

The mineral is distributed mostly in homogeneous globules. Some of them contain very small flame-like or lamellar inclusions of pentlandite seen only at great magnifications (Plate 4, Figure 2). Pyrrhotite-chalcopyrite intergrowths also occur. Chalcopyrite usually forms rims around pyrrhotite globules, but sometimes is the predominant phase with small inclusions of pyrrhotite.

The compositions of the pyrrhotite grains are notable for their high sulfur contents and rather low concentrations, up to 0.1 per cent of copper and up to 0.6 per cent of nickel (Table 5). High sulfur contents are borne out by X-ray powder diagrams which give a very small values for the d_{102} reflections (2.060Å). The pyrrhotite grains display monoclinic symmetry that was initially confirmed by magnetic suspension.

Chalcopyrite

This mineral occurs much less frequently than pyrrhotite. It occurs in intergrowth with pyrrhotite or in homogeneous grains. The homogeneous grains are sometimes euhedral, as opposed to pyrrhotite, and contain very small inclusions of a silicate mineral. Unlike pyrrhotite, the chalcopyrite varies significantly in composition (Table 5). Chalcopyrite from intergrowths with pyrrhotite has a constant composition similar to most common chalcopyrite. Copper content in it is not less than 31 per cent (recalculated to 100%); nickel concentration does not exceed 1 per cent, and its iron content is rather high, 32 to 33 per cent.

A second, rarer group of Cu-Fe-sulfides was discovered during microprobe investigations. Their composition is similar to cubanite. Results of the analyses of three cubanite grains (Table 5, Analyses 21 to 25) indicate much higher Ni-content than in chalcopyrite. Two of the cubanite grains have compositional homogeneity (Analyses 21 and 25), while the third is rather variable (Analyses 22 to 24). High copper (15.5 to 25.2%) and nickel (6.4 to 12.5%) content is found in a grain of Cu-Ni-sulfide in Sample 417D-69-1, 142 cm (Table 5, Analyses 12 to 15). These compositions appear to be Ni-rich intermediate solid solutions.

Pentlandite

The mineral forms very small ($\sim 1 \mu\text{m}$), flame-like lamellar inclusions in pyrrhotite grains (Plate 4, Figure 2). We were unable to conduct microprobe analyses of pentlandite because of its small size, but the diagnosis is fully predictable. Some globules contain all three sulfide minerals: pyrrhotite, chalcopyrite, and pentlandite.

Compositions of primary sulfides from oceanic basalts have significant differences according to various researchers (e.g., Czamanske and Moore, 1977; MacLean, 1977a, b). Distinctions in iron sulfide compositions are especially notable. Basaltic glass from the FAMOUS area contains monosulfide solid solution minerals (Czamanske and Moore, 1977) with low sulfur content (36 to 37%), and high

TABLE 5
Microprobe Analyses of Magmatic Sulfides

Sample (Interval in cm)	Analyses No.	Mineral ^a	Fe	Cu	Ni	S	Total
417D-69-1, 142	1	Po - 1	57.3	0.14	0.61	39.0	97.05
	2	Cp - 1	29.0	30.4	0.88	32.0	92.37
	3	Po - 2	57.7	0.08	0.63	39.0	97.4
	4	Cp - 2	30.3	32.4	0.85	34.2	97.84
	5	Po - 3	58.1	—	0.6	39.1	97.8
	6	Cp - 3	30.9	32.0	0.8	33.6	97.4
	7	Po - 4	60.0	—	0.1	40.6	100.7
	8	Cp - 4	31.7	30.5	6.61	36.3	99.11
	9	Po - 5	59.9	—	0.11	40.2	100.2
	10	Cp - 5	31.1	32.2	1.0	34.6	98.9
	11	Po - 6	60.3	—	0.23	40.0	100.5
	12	Iss - 7	31.6	25.2	6.4	36.0	99.2
	13	Iss - 7	30.7	23.9	7.9	34.4	96.8
	14	Iss - 7	37.9	15.5	9.5	36.2	99.1
	15	Iss - 7	30.2	17.0	12.5	34.5	94.2
418A-85-1, 33	16	Po - 1	58.1	0.06	0.3	39.8	98.2
	17	Po - 2	58.0	0.16	0.4	39.7	98.1
	18	Cp - 2	31.6	31.8	0.85	35.2	99.45
	19	Cp - 3	32.8	30.7	0.9	35.8	99.7
	20	Cp - 4	32.6	30.3	0.83	34.4	98.1
	21	Cb - 5	37.3	23.0	2.6	36.6	99.5
	22	Cb - 6	37.0	24.2	3.3	36.1	100.6
	23	Cb - 6	34.1	27.5	2.0	36.1	99.7
	24	Cb - 6	38.7	20.1	4.2	36.6	99.6
	25	Cb - 7	41.4	20.8	2.0	35.4	99.6

^aPo = pyrrhotite, Cp = chalcopyrite, Iss = intermediate solid solution, and Cb = cubanite; the numerals with the mineral symbols are identification numbers of analyzed grains consisting of either homogeneous minerals or sulfide intergrowths.

Ni (3.4 to 17.1%) and Cu (0.55 to 2.73%). Mathez (1976) has described similar monosulfide solid solution minerals from Pacific basalt glass. Pyrrhotite with high sulfur content (not less than 39%), and low Ni (0 to 1.5%) and Cu (0 to 0.2%), occurs in glass and fine-grained basalts of Leg 37 (MacLean, 1977a, b). There are also differences in Cu-Fe-sulfides. FAMOUS basalts contain intermediate solid solution minerals with 20 to 33 per cent Cu, 33 to 43 per cent Fe, and 0.9 to 2.3 per cent Ni, while MAR basalts of Leg 37 have variable intermediate solid solution minerals side-by-side with chalcopyrite with low Ni-content. The main reason for all these differences, evidently, is variation in rates of basalt solidification. Sulfides of coarse-grained basalts from Holes 417D and 418A are most similar to sulfides of Leg 37 basalts which crystallized at rather slow cooling rates. Re-equilibration could occur under subsolidus conditions causing intermediate and monosulfide solid solution minerals to be converted into pyrrhotite and chalcopyrite aggregates.

SECONDARY OPAQUE MINERALS

Pyrite

This, the most widespread of all sulfide minerals, develops with other alteration products in basalts. Pyrite forms predominantly homogeneous grains or aggregates, but locally occurs with marcasite and chalcopyrite in intergrowths. One can observe it in fine-grained basalt groundmass as small irregular distributed aggregates or, less frequently, as rather coarse grains (Plate 5, Figure 1) up to 1 mm across. Fine pyrite veinlets cut the groundmass and plagioclase or pyroxene phenocrysts (Plate 5, Figure 2). Its vesicle rims, filled with calcite (Plate 5, Figure 3) or smectite, are characteristic. Pyrite also replaces quartz in vesicles filled with calcite and surrounded with quartz rims (Plate 5, Figure 4). The mineral seems to be one of the latest

hydrothermal alteration products and is a common product of halmyrolysis. Compositions of studied pyrites are similar to the pyrites described by MacLean (1977) from MAR basalts of Leg 37. The principal minor elements are Ni and Co (usual 0.03 to 0.1%). Uneven distribution of these elements is peculiar. Pyrite rims (Plate 5, Figure 3), for example, have a zonality in Ni and Co contents as is demonstrated by X-ray scans (Plate 6, Figure 1a, b). Concentrations of Ni and Co in some places reach 0.53 and 0.43 per cent, respectively.

Marcasite

The mineral occurs much less often than pyrite, and forms growths with it. These growths are composed of minute grain aggregates. The grain texture of marcasite is demonstrated at crossed nicols due to anisotropy of the mineral.

Chalcopyrite

Secondary chalcopyrite occurs in altered basalts in close assemblages with pyrite, but in lesser quantities. It forms locally minute inclusions and growths with pyrite in basalt groundmass. Rare, larger aggregates of pyrite and chalcopyrite replace silicate minerals giving pseudomorphs (Plate 6, Figure 2). Chalcopyrite also occurs in thin rims around vesicles with calcite fillings (Plate 6, Figure 3). Dimensions of separate chalcopyrite grains reach to 100 to 150 μm (Plate 6, Figure 4a). They usually contain abundant minute inclusions of secondary silicates which cause microprobe analyses totals to be low. For example, analysis of the grain shown in Plate 6, Figure 4a, provides the following results: Cu = 32.6, Fe = 29.4, Ni = 0.06, Co = 0.03, and S = 33.5, for a total of 95.59 per cent. X-ray scans of the same grain (Plate 6, Figures 4b, c) demonstrate nickel-enrichment in its periphery similar to the pyrite grains. This enrichment seems to be caused by nickel extraction from rock-forming silicates during their interaction with solutions during alteration.

Iron Hydroxides

Found in Sample 417D-49-2, 82 cm, iron hydroxide aggregates are located in a celadonite veinlet as a chain of grains (Plate 7, Figure 1). In addition, they form pseudomorphs after parts of celadonite grains in basalt groundmass (Plate 7, Figure 2). Composition of the hydroxide from the veinlet is similar to the mineral composition from the groundmass (Table 6). Both analyses demonstrate a notable admixture of silica.

CONCLUSIONS

1. We have studied opaque minerals in 27 specimens of basalts recovered in Holes 417D and 418A. The most widespread primary ore mineral is titanomagnetite. There are also ilmenite, chromite, and sulfide globules occurring

in coarse-grained basalts. The predominant secondary opaque mineral is pyrite, which is accompanied sometimes by growths of chalcopyrite and marcasite. Iron hydroxides are also found.

2. Microprobe analyses of coexisting titanomagnetites and ilmenites indicate that the temperatures of formation and re-equilibration of these minerals lie between 1100° and 980°C.

3. Chromites found in a sample of coarse-grained basalt are highly variable in composition, even in adjacent grains. They are noted for higher $\text{Fe}^{3+}/\text{Fe}^{2+} + \text{Al} + \text{Cr}$ and lower $\text{Mg}/\text{Mg} + \text{Fe}^{2+}$ values, than Cr-spinels of the Leg 37 MAR basalts.

4. Compositions of the sulfide globules (consisting of monoclinic pyrrhotite, chalcopyrite, cubanite, and pentlandite) alongside coexisting titanomagnetite-ilmenite intergrowths and are indicative of rather slow cooling of the coarse-grained basalts containing them. Subsolidus conversions and re-equilibration-inducing exsolution of monosulfide and intermediate solid solution minerals and titanomagnetite took place in the rocks.

5. The latest hydrothermal and halmyrolysis alterations, performed intensively (especially in basalts with fine-grained groundmass), lead to formation of widespread pyrite mineralization.

REFERENCES

- Buddington, A.F. and Lindsley, D.H., 1964. Iron-titanium oxide minerals and synthetic equivalents, *J. Petrol.*, v. 5, p. 310-375.
- Carmichael, C.M., 1970. The Mid-Atlantic Ridge near 45°N. VII. Magnetic properties and opaque mineralogy of dredged samples, *Canadian J. Earth Sci.*, v. 7, p. 239-256.
- Carmichael, I.S.E., 1967. The iron-titanium oxides of salic volcanic rocks and their associated ferromagnesian silicates, *Contrib. Mineral. Petrol.*, v. 14, p. 36-64.
- Clarke, D.B. and Loubat, H., 1977. Mineral analysis from the peridotite-gabbro-basalt complex at Site 334, DSDP Leg 37. In Aumento, F., Melson, W.G., et al., *Initial Reports of the Deep Sea Drilling Project*, v. 37: Washington (U.S. Government Printing Office), p. 841-856.
- Czamanske, G.K. and Moore, J.G., 1977. Composition and chemistry of sulfide globules in basalt from the Mid-Atlantic Ridge rift valley near 37°N latitude, *Geol. Soc. Am. Bull.*, v. 88, no. 4, p. 587-599.
- Hall, J.M. and Fisher, J.F., 1977. Opaque mineralogy of basement rocks, Leg 37. In Aumento, F., Melson, W.G., et al., *Initial Reports of the Deep Sea Drilling Project*, v. 37: Washington (U.S. Government Printing Office), p. 857-874.
- Irvine, T.N., 1967. Chromian spinel as a petrogenetic indicator. Part 2. Petrologic applications, *Canadian J. Earth Sci.*, v. 4, p. 71-103.
- MacLean, W.H., 1977a. Sulfides in Leg 37 drill core from the Mid-Atlantic Ridge. *Canadian J. Earth Sci.*, v. 14, p. 656-683.
- _____, 1977b. Sulfides in the core from Leg 37 drill holes. In Aumento, F., Melson, W.G., et al., *Initial Reports of the Deep Sea Drilling Project*, v. 37: Washington (U.S. Government Printing Office), p. 875-882.
- Mathez, E.A., 1976. Sulfur solubility and magmatic sulfides in submarine basalt glass, *J. Geophys. Res.*, v. 81, p. 4269-4276.
- Poltavets, J.A., 1975. The discussion of Buddington-Lindsley titanomagnetite geothermometer on the basis of comparative analysis of the equilibrium of magnetite serie spinels, *Izvestia of the USSR Acad. of Sci.*, ser. geol., p. 63-72.

TABLE 6
Microprobe Analyses of Iron Hydroxides

	Fe ₂ O ₃	V ₂ O ₅	Al ₂ O ₃	MgO	MnO	CaO	SiO ₂	Total
Veinlets	76.3	0.11	0.89	1.0	0.09	0.33	7.3	86.02
Groundmass	75.4	0.18	0.83	1.0	0.08	0.49	6.5	84.38

Sigurdsson, H., 1977. Spinels in Leg 37 basalts and peridotites: phase chemistry and zoning. In Aumento, F., Melson, W.G., et al., *Initial Reports of the Deep Sea Drilling Project*, v. 37: Washington (U.S. Government Printing Office), p. 883-892.

Symes, R.F. and Bevan, J.C., Hutchison, R., 1977. Phase chemistry studies on gabbro and peridotite rocks from Site 334,

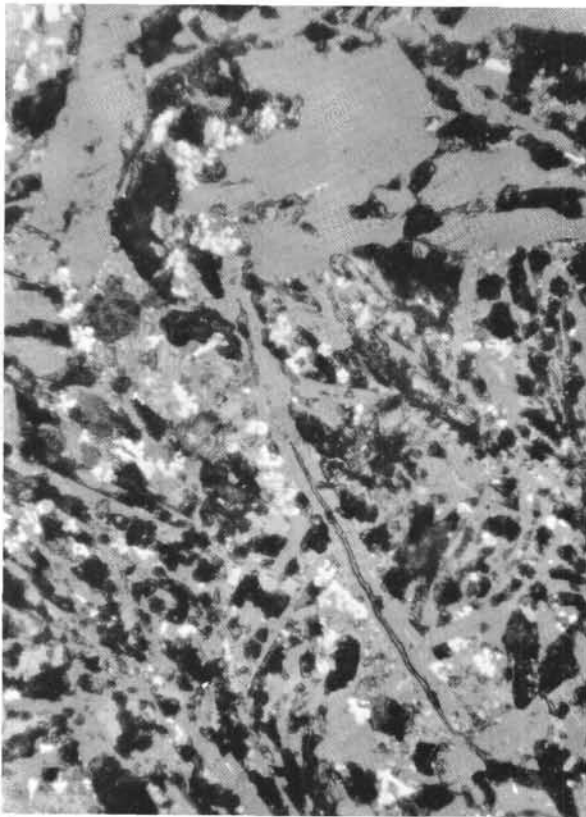
DSDP Leg 37. In Aumento, F., Melson, W.G., et al., *Initial Reports of the Deep Sea Drilling Project*, v. 37: Washington (U.S. Government Printing Office), p. 841-846.

Wayman, M.L., and Evans, M.E., 1977. Oxide microstructures and the magnetic properties of Leg 37 basalts, *Canadian J. Earth Sci.*, v. 14, p. 656-663.

PLATE 1

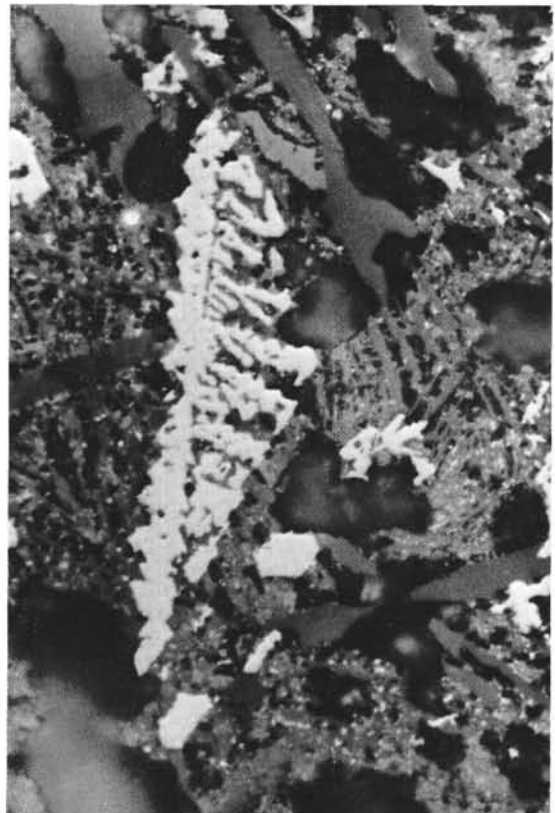
- Figure 1 Minute skeletal grains of titanomagnetite (white).
Sample 417D-49-2, 82 cm.
- Figure 2 Dendritic-skeletal form of a coarser grain and minute
point grains of titanomagnetite. Sample 417D-49-2,
82 cm.
- Figure 3 Minute point grains of titanomagnetite in mesostasis
of coarse-grained basalt. Sample 418A-79-1, 113 cm.
- Figure 4 Forms of minute titanomagnetite grains in mesostasis
of coarse-grained basalt. Sample 418A-79-1, 113 cm.

PLATE 1



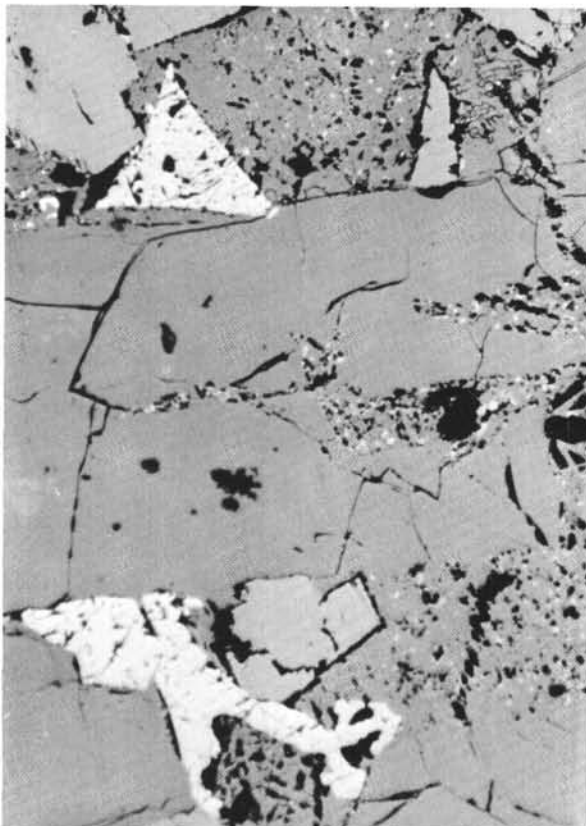
1

100 μ m



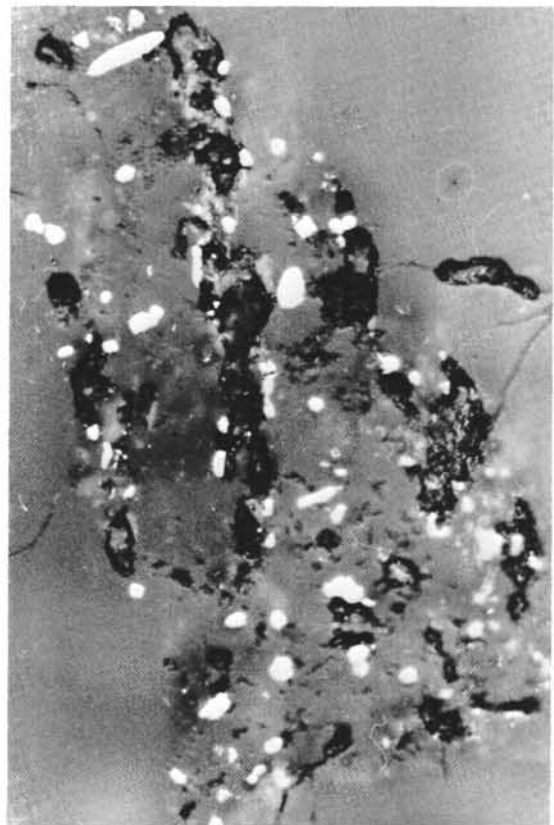
2

12.5 μ m



3

100 μ m



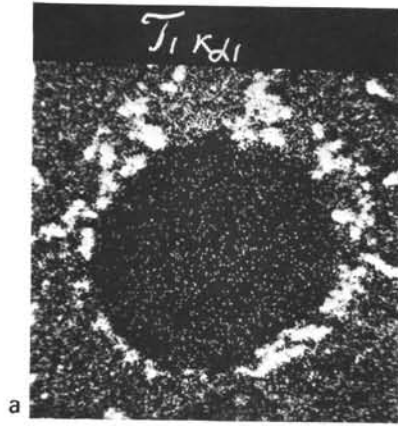
4

12.5 μ m

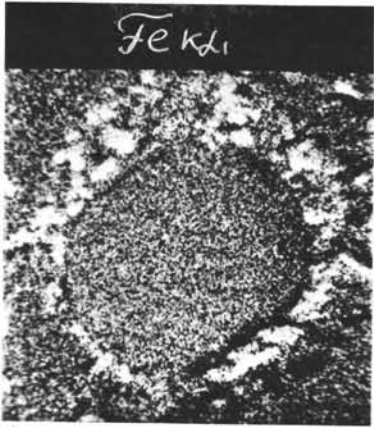
PLATE 2

- Figure 1 X-ray scans of $Ti_{K\alpha_1}$ (a) and $Fe_{K\alpha_1}$ (b) showing the distribution of titanomagnetite around a vesicle. $150\times$, $150\ \mu\text{m}$. Sample 417D-59-3, 104 cm.
- Figure 2 Coarse grains of titanomagnetite (white) and small sulfide globules in coarse-grained basalt. Sample 418A-79-6, 60 cm.
- Figure 3 A big skeletal titanomagnetite grain (white) in mesostasis of coarse-grained basalt. Sample 417D-69-1, 142 cm.
- Figure 4 A skeletal titanomagnetite grain (white) with minute sulfide globules adhered to it. Sample 417D-69-1, 142 cm.

PLATE 2

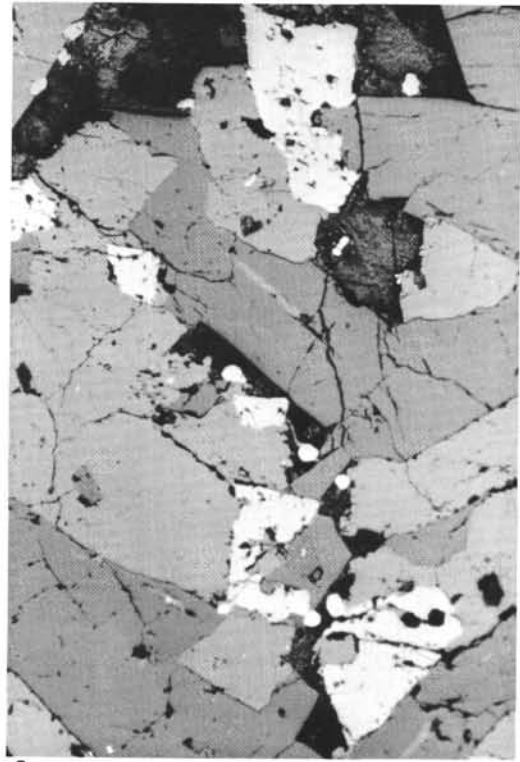


a



b

1



2

100 μ m



3

100 μ m



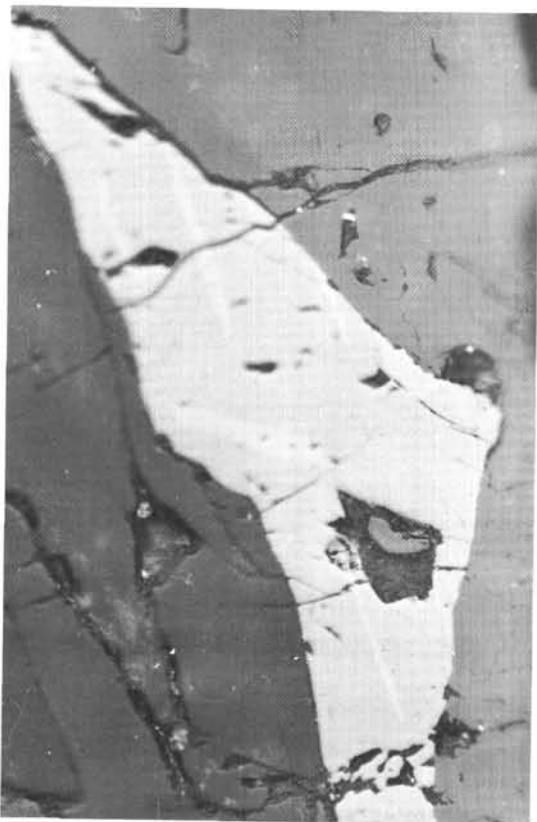
4

15.5 μ m

PLATE 3

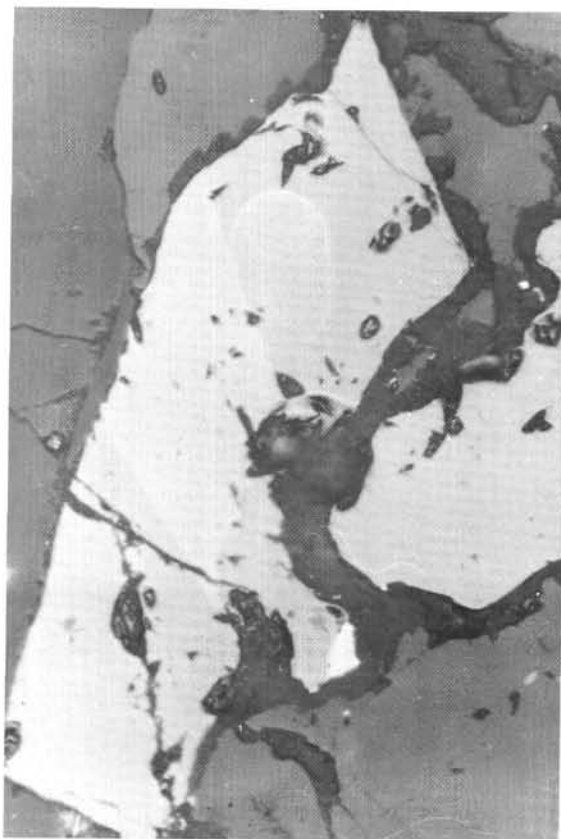
- Figure 1 Ilmenite lamellae (white) in the grain of titanomagnetite (gray). Sample 417D-69-1, 142 cm.
- Figure 2 A big ilmenite lamella (white) in titanomagnetite (gray). Sample 418A-85-1, 33 cm.
- Figure 3 Thin ilmenite lamellae (white) in titanomagnetite. Sample 418A-85-1, 33 cm.
- Figure 4 Chromospinel grains in smectite (Sm), replacing olivine (Ol). Spinel grains listed in Table 4 are marked with arabic numerals. Sample 418A-85-1, 33 cm.

PLATE 3



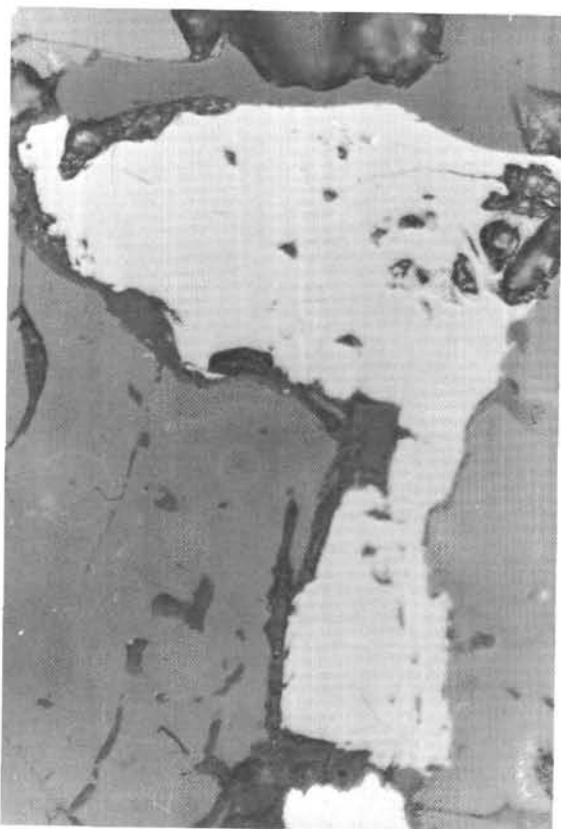
1

20µm



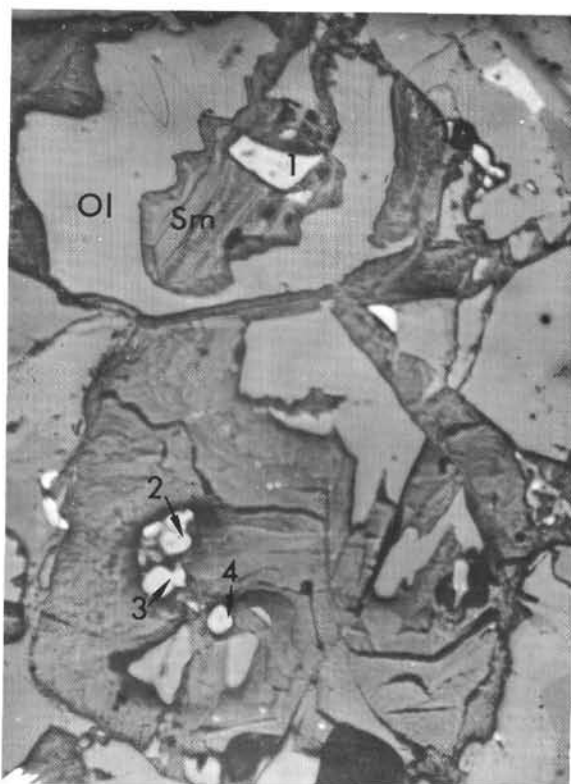
2

12.5µm



3

12.5µm



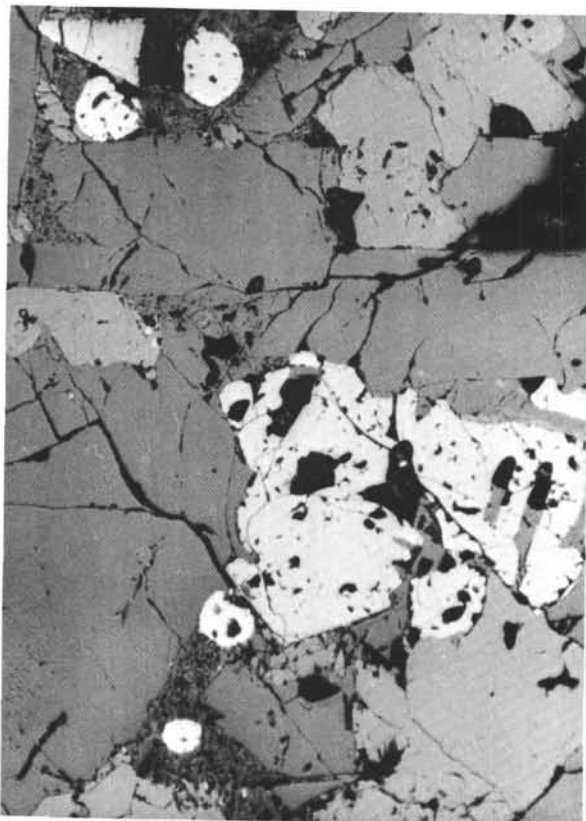
4*

100µm *

PLATE 4

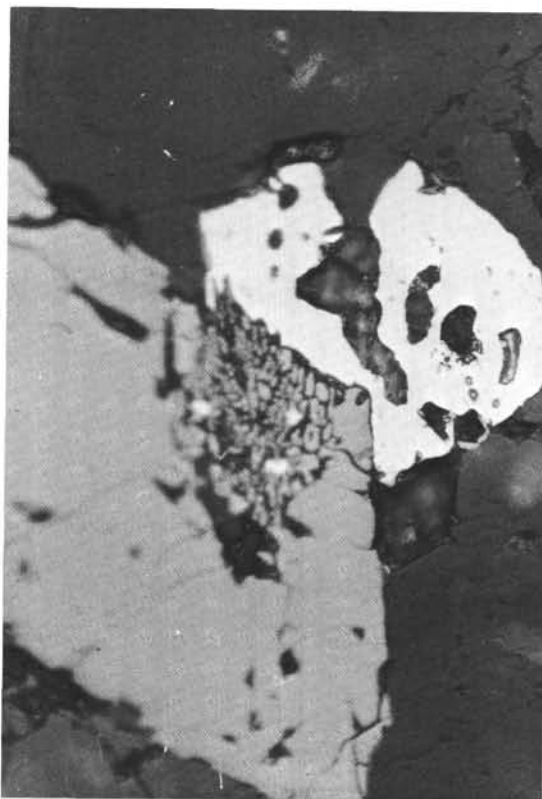
- Figure 1 Pyrrhotite globules and a large titanomagnetite grain. Sample 417D-69-1, 142 cm.
- Figure 2 An ellipsoidal grain of pyrrhotite with flame-like and lamellar inclusions of pentlandite. Sample 418A-85-1, 33 cm.
- Figure 3 Pyrrhotite (white) with glass inclusions overgrowing a grain of titanomagnetite (gray). Sample 417D-69-1, 142 cm.
- Figure 4 An overgrowth of pyrrhotite (white) and titanomagnetite with ilmenite lamellae. Sample 418A-85-1, 33 cm.

PLATE 4



1

100 μ m



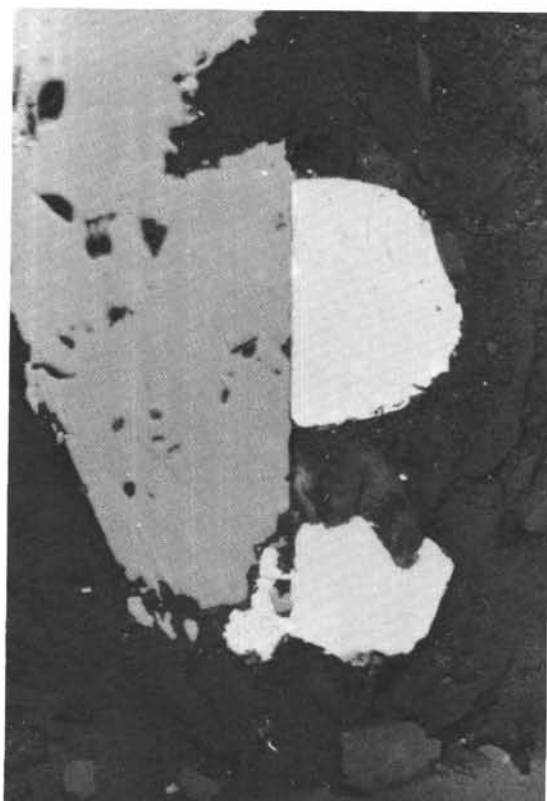
2

20 μ m



3

12.5 μ m



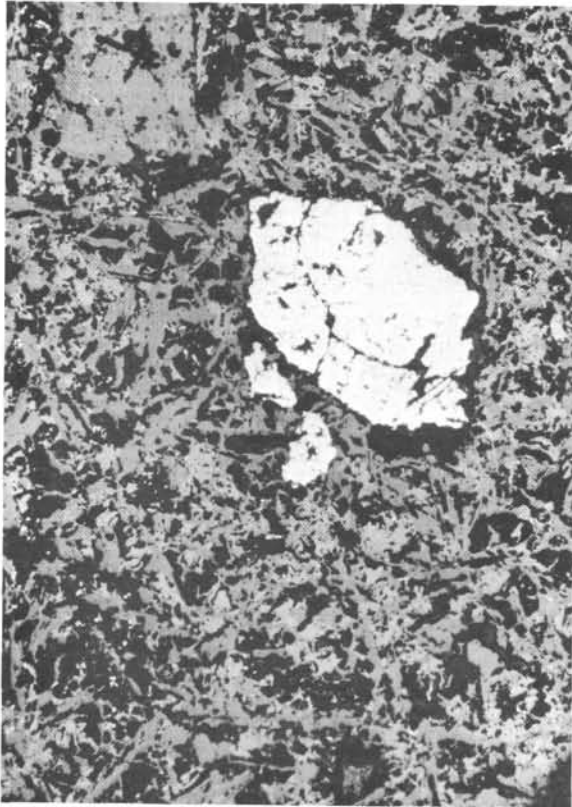
4

12.5 μ m

PLATE 5

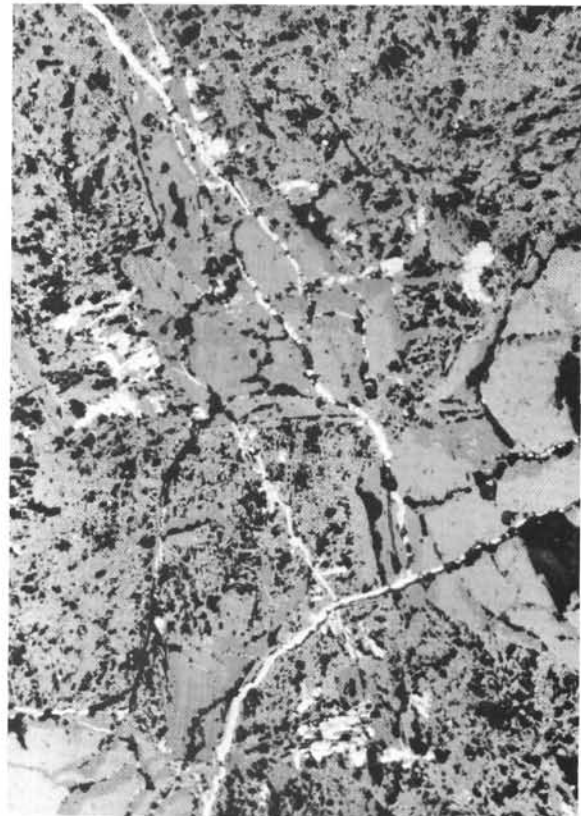
- Figure 1 Pyrite (white) in basalt. Sample 417D-52-4, 13 cm.
- Figure 2 Pyrite veinlets (white) in basalt. Sample 417D-59-3, 104 cm.
- Figure 3 A pyrite rim (white) around a carbonate-filled vesicle in basalt. Sample 417D-52-4, 13 cm.
- Figure 4 Pyrite (white) replacing a quartz rim around a calcite-filled vesicle in basalt. Sample 418A-58-4, 143 cm.

PLATE 5



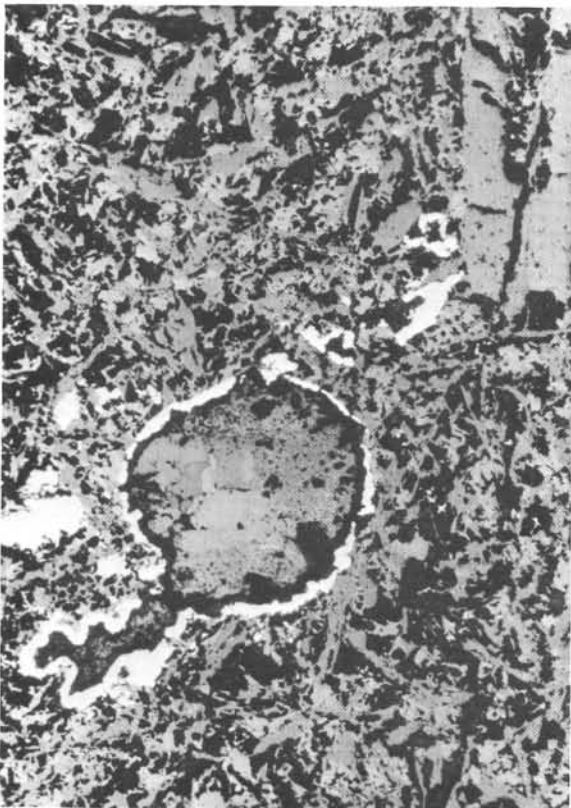
1

100μm



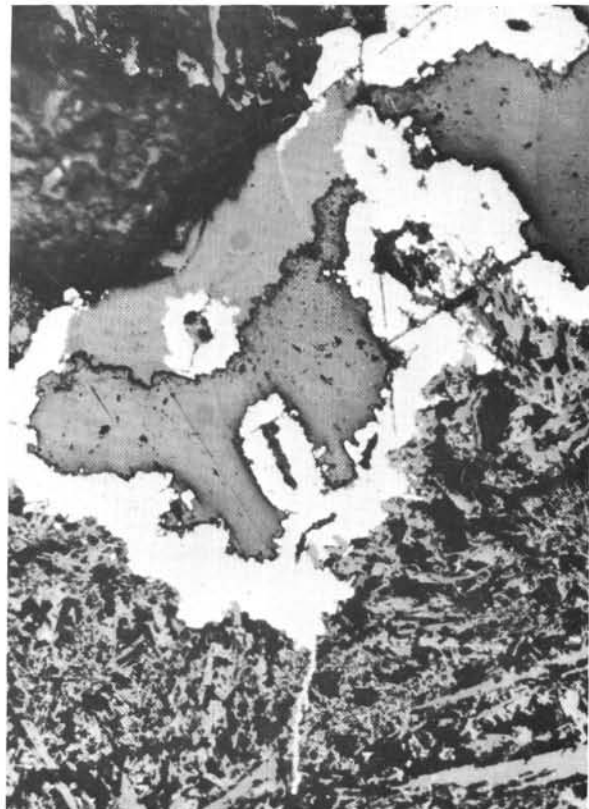
2

100μm



3

100μm



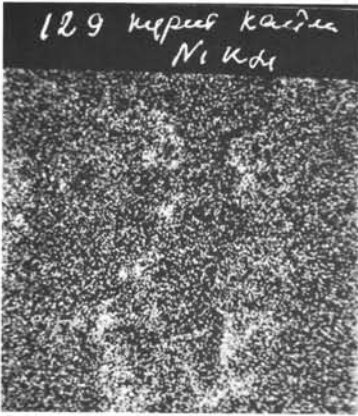
4

100μm

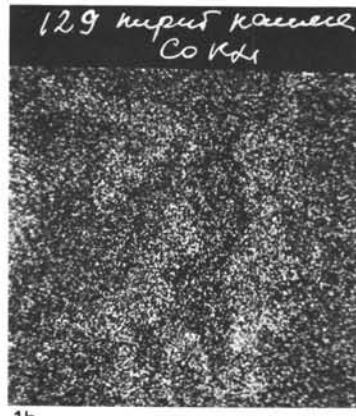
PLATE 6

- Figure 1 X-ray scans of the pyrite rim shown in lower left-hand corner of Plate 5, Figure 3; a= $\text{NiK}\alpha$; b= $\text{CoK}\alpha$. 250 \times , 250 μm . Sample 417D-52-4, 13 cm.
- Figure 2 Intergrowths of chalcopyrite (1) and pyrite (2) in basalt. Sample 417D-59-3, 104 cm.
- Figure 3 A chalcopyrite rim (white) around a smectite-filled vesicle. Sample 417D-59-3, 104 cm.
- Figure 4 A chalcopyrite grain (white) (a) and its X-ray scans, (b) $\text{NiK}\alpha$ and (c) $\text{CoK}\alpha$. 100 \times , 100 μm . Samples 417D-69-1, 142 cm.

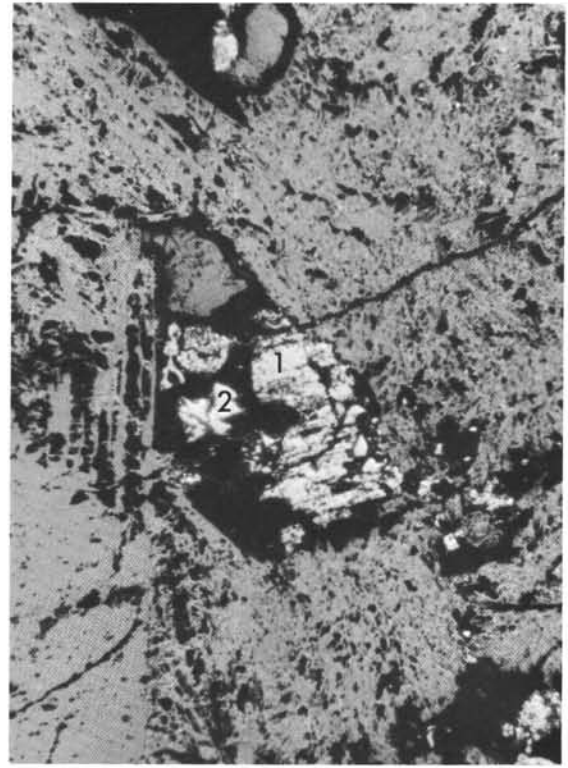
PLATE 6



1a

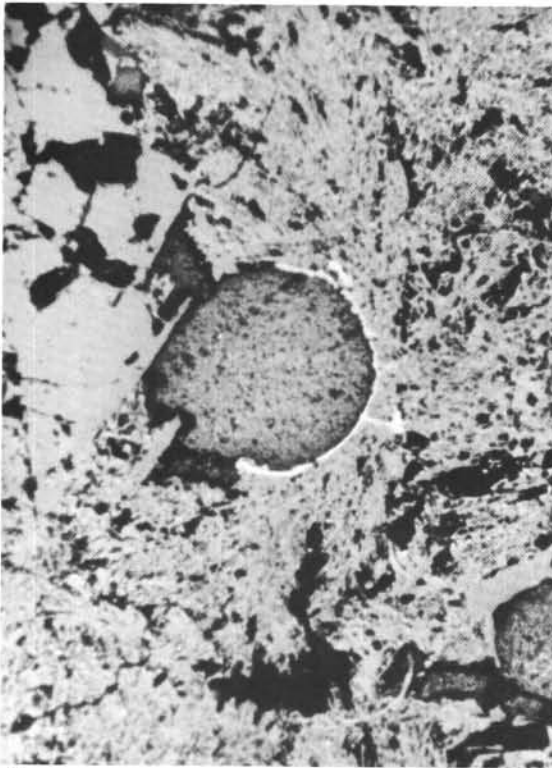


1b



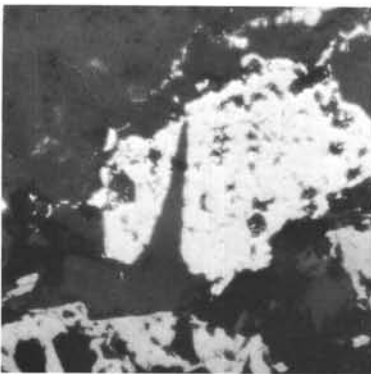
2

77μm

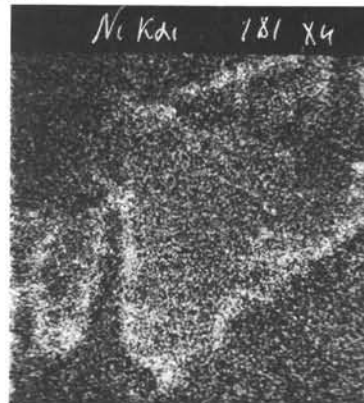


3

62μm



4a



4b



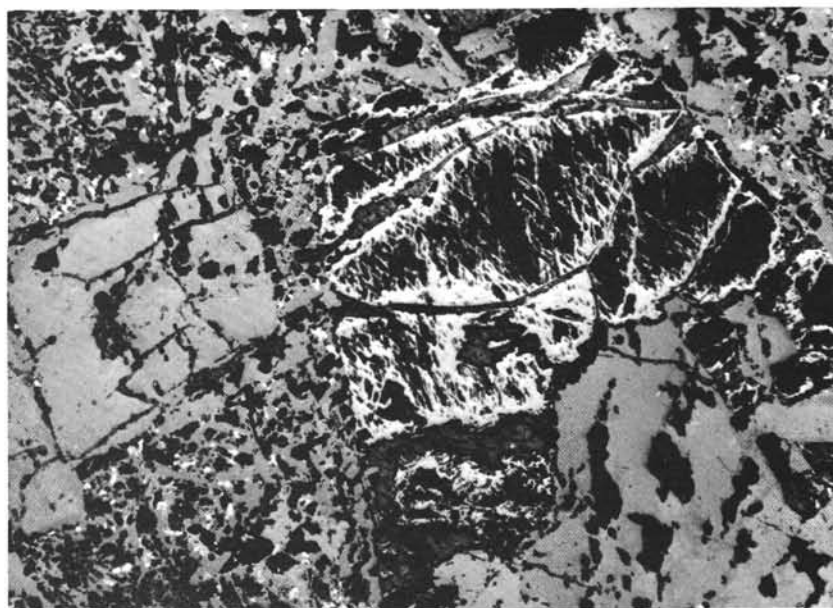
4c

PLATE 7



1

100 μ m



2

100 μ m

Figure 1 Iron hydroxides (light gray) in a celadonite-filled veinlet in basalt. Sample 417D-49-2, 82 cm.

Figure 2 Iron hydroxide pseudomorphs after smectite. Sample 417D-49-2, 82 cm.